Part II

Our Applications

Chapter 9

Diameter Measurement of Cylindrical Objects

9.1 Introduction

9.1.1 Initial context: measurement in forest surveying

The computerization of the diameter measurement of the trees in our forests, as a part of the "hammering" process, preceding the cutting down or for inventory purposes, is one of today's challenges of forest surveying. The present most advanced technique is to record measurements on the spot, using an electronic forest caliper, avoiding in such a way to manually encode the results, which is a possible source of error.

The usual instrument is of the sliding-rule type (see Fig. 9.1); the disadvantages of this instrument are to be found in the mobile mechanical part, unavoidably leading to wear and fouling, and in the fact that it requires both hands to be carried.

Fig. 9.1. Electronic caliper. Sliding-rule type.

In order to overcome these limitations, our laboratory created a first new caliper based on ultrasonics [41] a few years ago (see Fig. 9.2). Its differences with the other existing calipers were that it contained no mobile component and that it could be handled with one hand only. The other was then free to carry out hammering operations or to encode secondary data on the keyboard such as the species of the tree, the parcel number...

One drawback was still present, as it was for all the other calipers: a contact between the apparatus and the tree was necessary. In order to gain in comfort and efficacy, we studied the feasibility of applying laser triangulation under structured lighting for the diameter measurement. This method would allow us to work at a distance and to overcome most of the weaknesses of the previous caliper.

Fig. 9.2. Electronic caliper based on ultrasonics.

9.1.2 Generalization to the diameter measurement of cylindrical pieces

This chapter presents the developments and conclusions of this study which, it is important to notice, commonly applies to the diameter measurement of random cylindrical pieces. It considerably enlarges the field of use of the instrument to any ambulatory industrial application where a noncontact diameter measurement of a cylinder is needed.

As examples, let us cite the following applications:

- detection and shape characterization of obstacles and other mechanical pieces in the robotic inspection field;
- diameter measurement of pipes of difficult access (because of their position, their temperature...) in industrial sites;
- quality control in the building sector when columns or other cylindrical pieces are to be measured.

In the forest surveying field, the maximum allowed error on the diameter is of 1%, the diameter range being of 10–50 cm [41]. As this device is the first to propose a noncontact solution for the measurement of trunks, there is no standard regarding the operating distance between the instrument and the object. We thus decided of our own objective, which is to consider a distance range of 0.5–2 m. The figures in this paragraph summarizes the performances to be achieved by our instrument.

Note that in [42], a different approach for the forest inventories is presented. Working at large distance and using laser scanning, the technique consists in analyzing 3-D maps where several trunks appear. Segmentation algorithms allow to identify to which tree each 3-D point is belonging, and a cylinder fitting procedure applied on each group of points lead to the diameters. Unfortunately, the achievable accuracy is only of 10%.

9.1.3 Organization

For sake of clarity, we chose to organize this chapter as progressively evolving from the simplest situation to more elaborated ones. It will allow us to progressively introduce the concepts involved in this application, to end up with a general and efficient system. (This actually follows the same chronological order as the study we made.)

As a first step, we consider the case of a cylinder whose axis is perpendicular to the camera plane (Section 9.2). This simple problem was the starting point of the study [43].

After a short description of the image processing algorithm (Section 9.3), a presentation of the "three-tangent method," used for the radius calculation, is given in Section 9.4. We prove—Section 9.5—that it is the most reliable way of solving the problem, taking into account the particular characteristics of the laser curve.

In Section 9.6, we show that unacceptable errors can be committed if the cylinder slant is not taken into account, for nontransversal aims.

This observation naturally led us to improve our method for allowing the diameter measurement of randomly tilted cylinders (Sections 9.7 to 9.10).

In Section 9.11, we calculate the error that one can expect on the radius, using the accuracy analysis of Chapter 7.

We finally show the experimental results we obtained on a pre-prototype setup (Section 9.12), explain what would have occurred if our theoretical models were not so refined (Section 9.13), and give some conclusions (Section 9.14).

Note that the present chapter groups and develops three papers previously published [44] [45] [46].

9.2 Case of a Cylinder Transversal to the Camera Plane

Let the cylinder under test have its axis perfectly perpendicular to the $(x,\ y)$ plane of a monochrome CCD camera observing the scene (Fig. 9.3). Systems of reference (x, y, and z) and (x_{pix}, y_{pix}) are as defined in Chapter 2. For convenience, the camera plane will often be represented as horizontal, but of course is it not mandatory.

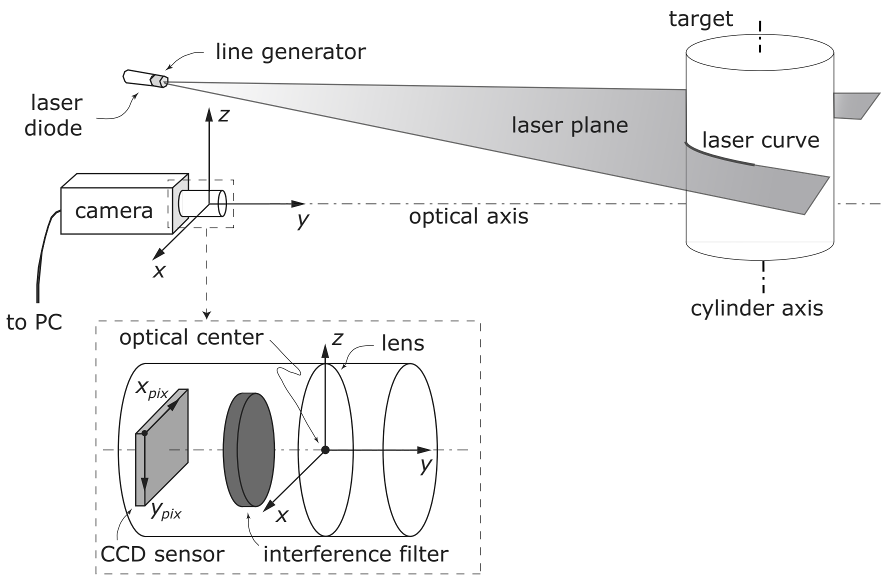

Fig. 9.3. Configuration of the device. 3-D view. Case of a transversal aim.

The object, supposed perfectly cylindrical, is illuminated by a laser plane slightly tilted in the y direction on the camera plane, creating a curved line on the object. We will further see that more planes are needed in the general case of a randomly tilted cylinder.

We suppose that the portion of the cylinder illuminated by the laser plane is at least equal to that seen by the camera. A satisfactory way of complying with that condition is to set the diode a little bit back from the camera. The surface of the object is supposed at least partially diffusing, so that in any case, the camera receives a part of the plane luminance.

As described in Chapter 4, a narrow-band interference filter, centered on the wavelength of the laser diode, is placed between the CCD sensor of the camera and its objective, in order to increase the contrast between the curve to be extracted and the rest of the scene.

The main advantage of the structured lighting method for this particular application is permitting in one operation only, the evaluation of both the distance D between the target and the optical center of the camera [by triangulation in the vertical plane, cf. Fig. 9.4(a)] and the angular aperture τ under which the object is seen [the width of the laser curve in the ICS is an image of it, cf. Fig. 9.4(b)]. These two measurements lead to the radius R of the cylinder. It is to be noted that to make these two features more "visible", Fig. 9.4 shows the case of a centered aim at the cylinder, but this restriction is not supposed in the study hereafter.

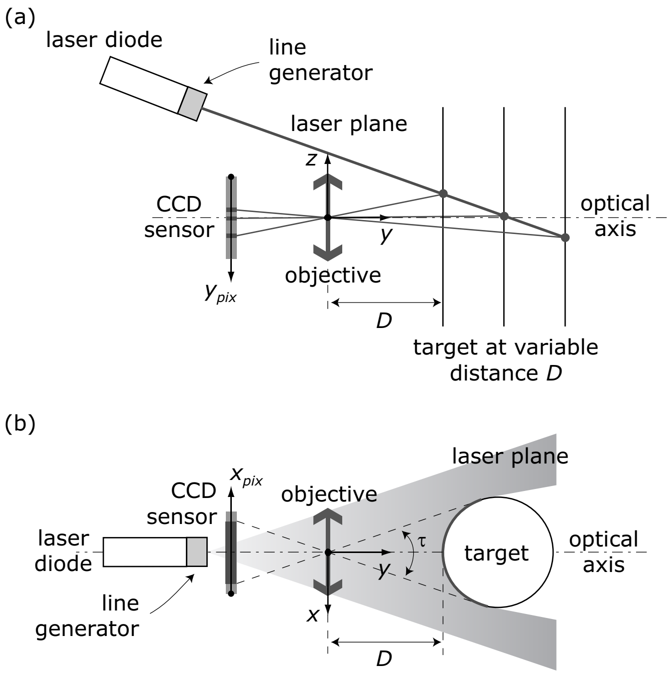

Fig. 9.4. (a) View in a vertical plane: D measurement by triangulation. (b) View in an horizontal plane: angular aperture τ measurement.

Our instrument is defined by ten parameters: seven for the camera (see Chapter 2) and three for the laser plane (see Fig. 9.5 and Section 3.5). Distance e is intentionally limited to about 10 cm to maintain the compactness and the ambulatory nature of our instrument. Tilt angle δ and the zoom factor of the camera (adjusted mainly by changing the focal length) are chosen so that the instrument covers the distance and radius ranges for the concerned application (i.e. the laser line must stay in the field of view of the camera in any case). For additional interpretation of Fig. 9.5, see also Fig. 9.7.

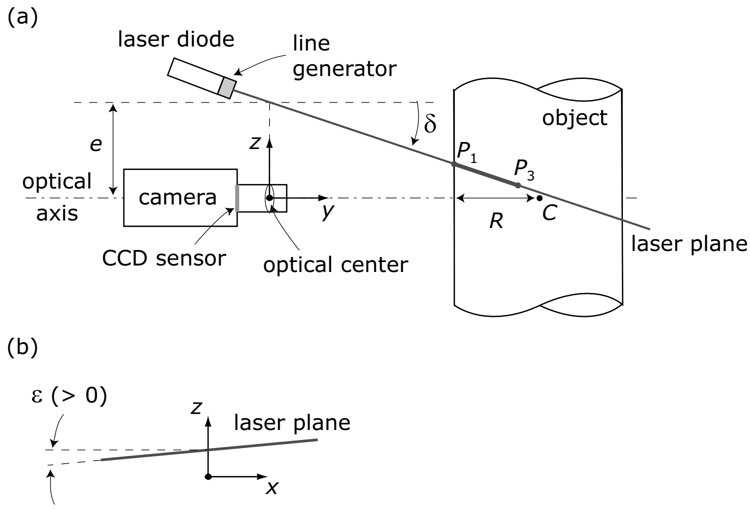

Fig. 9.5. Geometry of the device. (a) Cut in the vertical plane (y, z). (b) Cut in the vertical plane (x, z).

The two distinct procedures described in Chapter 6 are used to calibrate the instrument, the laser plane calibration being performed on known cylindrical objects (even though mentioned here, the latter can obviously not be performed until the radius calculation method has been chosen; see Section 9.4).

9.3 Image Processing

An image processing algorithm extracts the laser curve intersected by the cylinder by isolating it from the rest of the scene. The interference filter carries out a substantial part of the task, but some additional treatments on the image are still needed to eliminate the noise surrounding the curve.

These are (see Chapter 5 for a description of each item):

- subtraction of two pictures sequentially taken (one with the laser diode on, the other with the diode off);
- thresholding;
- segmentation;
- laser curve selection;
- column-by-column subpixel location of the curve;

- curve smoothing;
- correction of the distortion.

9.4 Radius Calculation: the "Three-Tangent Method"

As shown in Chapter 3, a one-to-one correspondence exists between the ICS coordinates of any pixel of the laser curve and the WCS coordinates of the corresponding point in the scene.

We can thus assess that the coordinates of every point of the laser curve are known in the WCS by (3.7). The accuracy that we can achieve on these coordinates however depends on the position these points are occupying on the curve, as we will show later.

The projection, onto the camera plane, of the intersection of the laser plane with the cylinder is a circle. The radius calculation is performed by mean of what we call the "three-tangent method," a patented [47] method based on the property that a circle is entirely defined by three of its tangents. We will later justify the choice of this method in comparison with others available to reconstitute a circle.

In fact, three secant right lines define four circles to which these lines are tangent, but the pertinent circle in our case is unambiguously the circle of center C that the camera's optical axis is aiming at (see Fig. 9.6).

The specific tangents we chose are OP_2, OP_3 and $P_1P_{3'}$, the latter being parallel to axis x (cf. Fig. 9.7, where—it is important to notice—we supposed an uncentered aim). Their knowledge only demands the determination of:

- distance Y_1, i.e. the ordinate of the closest point (belonging to the target) to the operator (in the y direction);
- abscissas $X_{2'}$ and $X_{3'}$ of the two extreme points (i.e. intersecting the two other tangents) of tangent $P_1P_{3'}$. We suppose $X_{3'} > X_{2'}$.

Those two points are non-material, but their WCS coordinates can be deduced from P_2 and P_3 abscissas and P_1 ordinate in the ICS.

The radius R of the cylinder is inferred from those quantities Y_1, $X_{2'}$ and $X_{3'}$ as follows.

We begin with the equation of the circle, expressed from its center (X_1, $Y_1 + R$):

$$(x - X_1)^2 + (y - (Y_1 + R))^2 = R^2 \tag{9.1}$$

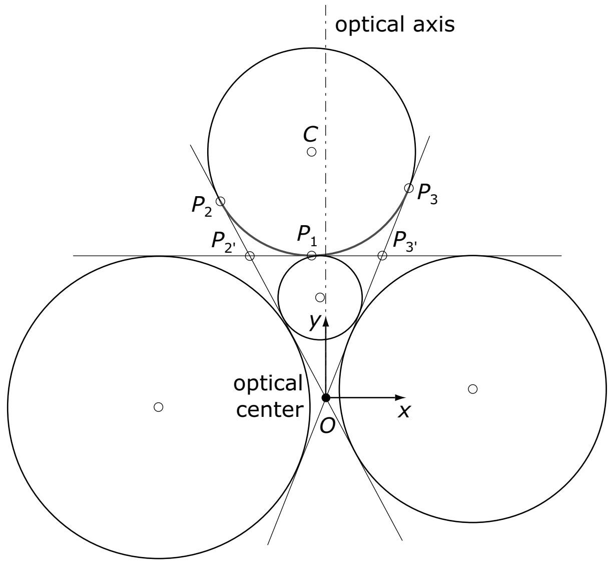

Fig. 9.6. "Three-tangent method." View in the camera plane: three right lines define four circles to which these lines are tangent.

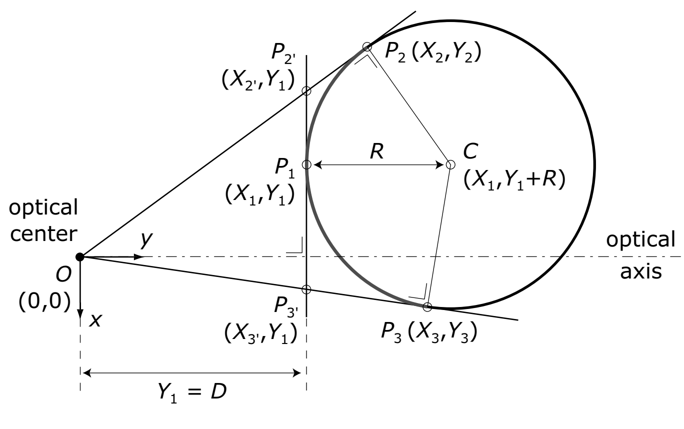

Fig. 9.7. "Three-tangent method." View in the camera plane: geometry of the problem.

The intersection between the circle and each of the two tangents OP_2 and OP_3 of equations

$$OP_2 \equiv y = \frac{Y_1}{X_{2'}}x \; ; \; OP_3 \equiv y = \frac{Y_1}{X_{3'}}x \tag{9.2}$$

gives a unique solution. Substituting y in (9.1) by its expression in formulas (9.2) provides us with two second-degree equations. Expressing that their determinants must be equal to zero gives us a system of two equations with two unknowns R and X_1:

$$\left\{ \begin{array}{lcl} X_1^2 Y_1 - 2X_1 X_{2'} (Y_1 + R) - Y_1 R^2 + X_{2'}^2 (Y_1 + 2R) & = & 0 \\ X_1^2 Y_1 - 2X_1 X_{3'} (Y_1 + R) - Y_1 R^2 + X_{3'}^2 (Y_1 + 2R) & = & 0 \end{array} \right. \tag{9.3}$$

whose partial resolution—X_1 is not determined—gives:

$$R = \frac{Y_1 (X_{3'} - X_{2'})}{\sqrt{X_{2'}^2 + Y_1^2} + \sqrt{X_{3'}^2 + Y_1^2} - (X_{3'} - X_{2'})} \tag{9.4}$$

9.5 Justification of the "Three-Tangent Method"

Analyzing the laser line in the image plane allows us to show why our method is the most suitable for computing the radius. Suppose a centered aim (the qualitative conclusions are still valid in the uncentered case). The laser curve in the WCS, projected onto the camera plane, has the equation (9.1) of the circle of Fig. 9.7 (in the centered case, with $X_1 = 0$)

$$x^2 + (y - (Y_1 + R))^2 = R^2 \tag{9.5}$$

limited to the left portion ending in P_2 and P_3, defined by the condition (ordinate of the tangency points):

$$y \leq \frac{Y_1 (Y_1 + 2R)}{Y_1 + R} \tag{9.6}$$

Using (3.7), we obtain the curve in the image plane (we supposed, without loss of generality $f_x = f_y$ and $\gamma = 0$):

$$x_{pix}^2 = -Y_1 (Y_1 + 2R) y_{pix}'^2 + 2f_y (Y_1 + R) y_{pix}' - f_y^2 \tag{9.7}$$

with $y_{pix}' = (y_{pix} + f_y \tan\delta)/e$ (shifted reduced ordinate), subject to the condition derived from (9.6):

$$y_{pix}' \leq \frac{f_y (Y_1 + R)}{Y_1 (Y_1 + 2R)} \tag{9.8}$$

An example of this curve is given in Fig. 9.8.

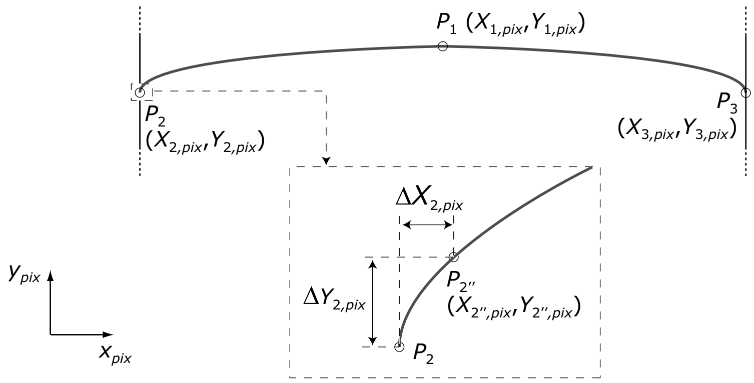

Fig. 9.8. Example of curve; view in the image plane; centered aim. Note that $X_{1,pix} = 0$, implying $X_{2,pix} = -X_{3,pix}$ and $Y_{2,pix} = Y_{3,pix}$.

The phenomenon at the basis of the choice of our method is the loss of the laser line luminance L, i.e. the information saved by the camera, near the tangency, as a consequence of the diffuse reflectance of the target (as supposed in Section 9.2).

Consider the ideal case of uniform diffusion, i.e. reflecting under constant luminance in any direction. By Lambert's law, L is proportional to the received illuminance E:

$$L = \rho E/\pi \tag{9.9}$$

where ρ is the object's reflectance.

As the laser plane is supposed of constant flux density along the intersection line, E is proportional to the cosine of the angle of incidence, which tends to zero under grazing incidence, with the same consequence for L.

One or more darker pixels are thus unavoidably cut from the curve ends during the image processing. The extreme points on which we work appear to be shifted to $P_{2''}$ and $P_{3''}$, introducing errors $\Delta X_{2,pix}$ and $\Delta Y_{2,pix}$ on tangency points P_2 and P_3 in the image plane (see Fig. 9.8).

We derive from (9.7) that dy_{pix}/dx_{pix} is infinite at the limits of the laser line as seen by the camera. (This result is rather obvious as the curve, for an hypothetical transparent cylindrical object, would close itself from these points, symmetrically to the part traced for the front of the object, implying therefore a vertical tangent at these limits). We will thus always have $\Delta Y_{2,pix} >> \Delta X_{2,pix}$. This implies considerable errors on Y_2 and Y_3, but also on X_2 and X_3, which depend on y_{pix} as well, as shown by (3.7).

On the other hand, the derivative dy_{pix}/dx_{pix} is equal to zero at the center of the curve, implying a good accuracy on Y_1, directly deduced from $Y_{1,pix}$, for which the resolution moreover is subpixel. If we relax the hypothesis of a centered aim, X_1 will be highly erroneous. Indeed, several central pixels will actually have the same ICS ordinate as P_1, due to the discrete character of the image. It will thus be difficult to exactly identify its abscissa $X_{1,pix}$. On the contrary, $X_{2'}$, found by (3.7) with $X_{2',pix} = X_{2,pix}$ and $Y_{2',pix} = Y_{1,pix}$, will have a noticeable accuracy. Actually, the relative error $\rho(X_{2'})$ on this abscissa is nearly equal to $\rho(X_{2,pix})$ as $Y_{1,pix}$ is negligibly erroneous. We thus have

$$\rho(X_{2'}) \cong \rho(X_{2,pix}) = \frac{\Delta X_{2,pix}}{X_{2,pix}} \tag{9.10}$$

which is very small. $X_{3'}$ obviously has the same property. TABLE 9.1 synthesizes all these comments.

TABLE 9.1. Accuracy on P_1, P_2, P_3, $P_{2'}$ and $P_{3'}$ coordinates. Y_1, $X_{2'}$ and $X_{3'}$ only are used in the "three-tangent method"

	Accuracy	**Justification**
Y_1	Very good	Nil derivative dy_{pix}/dx_{pix} at the center
X_1	Very bad	Nil derivative dy_{pix}/dx_{pix} at the center
Y_2 and Y_3	Very bad	Infinite derivative dy_{pix}/dx_{pix} at the extremes
X_2 and X_3	Very bad	Infinite derivative dy_{pix}/dx_{pix} at the extremes
$Y_{2'}$ and $Y_{3'}$	Very good	Same ordinate as P_1 $(= Y_1)$
$X_{2'}$ and $X_{3'}$	Good	One lost pixel has a minor influence [see (9.10)]

To conclude, our method perfectly circumvents the restrictions introduced by the general shape of the laser line viewed on the CCD sensor, as it relies only on partial coordinates accurately known. More classical methods, for instance based on the reconstruction of a circle from both coordinates of three of its points (explored in [43]), would not be robust, seen that for none of the laser curve point, both the abscissa and the ordinate could be determined with a satisfactory accuracy in the WCS. It would namely be the case if the three points were P_1, P_2 and P_3.

9.6 Error Made if the Cylinder Tilting is not Taken into Account

9.6.1 Preliminaries

The restriction of the method presented above is that the cylinder under test has to be standing perpendicularly to the camera plane.

In the perspective of enlarging the application field of the instrument in the industrial context, it is needed to generalize the method to the diameter measurement of cylinders of any orientation with respect to the measuring head.

Let the cylinder under test now have an arbitrary orientation defined by the angles (α, β)—elevation and azimuth—or, equivalently, (θ, φ)—defined in the planes (y, z) and (x, z)—with regard to the camera plane (see Fig. 9.9, where the origin of the WCS is placed on the cylinder axis only for readability).

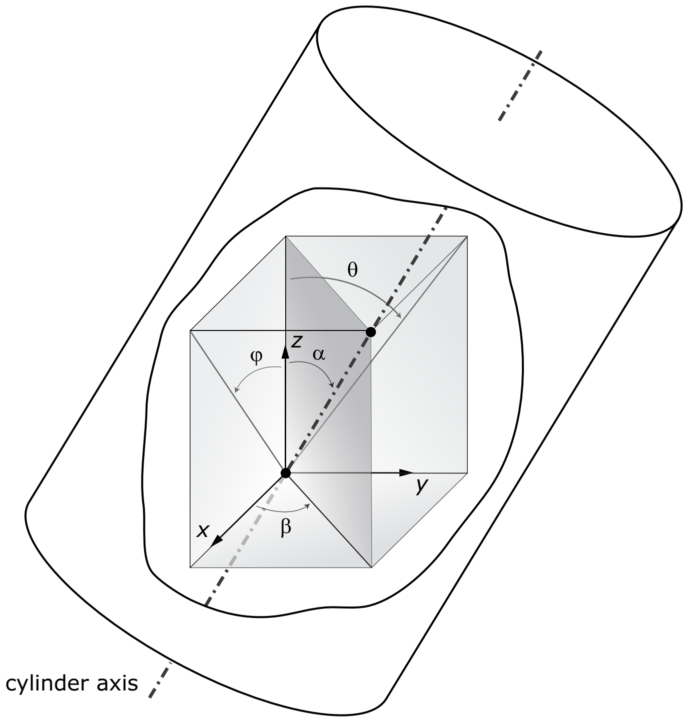

Fig. 9.9. Cylinder axis orientation. Angle θ is in the (y, z) plane, φ in the (x, z) plane, β in the (x, y) plane and α in the plane formed by z and the cylinder axis.

The relations between the two systems of orientation are:

$$\begin{cases} \tan^2\alpha = \tan^2\theta + \tan^2\varphi \\ \varphi \geq 0 \rightarrow \beta = \arctan\frac{\tan\theta}{\tan\varphi}\ ;\ \varphi < 0 \rightarrow \beta = \pi + \arctan\frac{\tan\theta}{\tan\varphi} \end{cases} \tag{9.11}$$

9.6.2 Methodology

In order to foresee the pertinence of such a generalization, *let us examine the error that is committed on the measurement when the cylinder slant is not taken into account for nontransversal aims.* It is to be noted that in this study, we suppose a centered aim (the qualitative results remain valid in the uncentered case).

To calculate the error, starting from the equation (9.5) of the cylinder in the WCS, we firstly have to find Y_1, $X_{2'}$ and $X3'$ necessary to the radius determination, and then to apply the "three-tangent method."

For sake of clarity, we have considered the two particular cases where only one of the angles (θ, φ), describing the object orientation, is different from zero.

9.6.3 Case 1: $\theta \neq 0$ and $\varphi = 0$

Let us start with a transversal aim at a cylinder, supposed of infinite length and described in the WCS by

$$(x - X_C)^2 + (y - Y_C)^2 = R^2 \tag{9.12}$$

where X_C and Y_C are the coordinates of the cylinder axis [(9.12) is a replica of (9.5)].

Rotating the camera by an angle θ around axis x implies the following transformation:

$$y \rightarrow y \cos\theta - z \sin\theta \tag{9.13}$$

As the latter does not alter the symmetry of the laser curve around the optical axis, X_C is set to zero, in order to simulate a centered aim. The cylinder equation thus becomes:

$$x^2 + (y \cos\theta - z \sin\theta - Y_C)^2 = R^2 \tag{9.14}$$

The expression of the intersection between the cylinder and the laser plane, projected onto the camera plane, is determined by equation (3.5) of the laser plane:

$$z = e - y \tan\delta \tag{9.15}$$

where we supposed $\epsilon = 0$, for sake of easiness. We thus have:

$$x^2 + (y(\tan\delta \sin\theta + \cos\theta) - e \sin\theta - Y_C)^2 = R^2 \tag{9.16}$$

Ordinate Y_1 of point P_1 is the value of this curve evaluated in $x = 0$, so that one can express Y_C as:

$$Y_C = Y_1(\tan\delta \sin\theta + \cos\theta) - e \sin\theta + R \tag{9.17}$$

and replace it in (9.16).

Abscissas $X_{2'}$ and $X_{3'}$ are at the intersection between the straight line $y = Y_1$ and the two tangents to the curve (9.16) passing by the origin of the WCS. Their equations are

$$y = \pm T_\theta x \tag{9.18}$$

where we have to calculate T_θ so that the determinant of (9.16), when having substituted y by (9.18) in this expression, is equal to zero. One easily finds:

$$T_\theta = \frac{Y_1}{R}\sqrt{1 - \frac{2R}{Y_1\left(\tan\delta\sin\theta + \cos\theta\right)}} \tag{9.19}$$

We then have:

$$X_{2'} = -\frac{Y_1}{T_\theta} \;;\; X_{3'} = \frac{Y_1}{T_\theta} \tag{9.20}$$

Expression (9.4) gives us the erroneous R_θ resulting from the "three-tangent method." The relative error ρ_θ made on the measurement is then:

$$\rho_\theta = \frac{R_\theta - R}{R} \tag{9.21}$$

It is symmetrical around $\theta = \delta$ and depends on R, Y_1, e and δ.

9.6.4 Case 2: $\theta = 0$ and $\varphi \neq 0$

In this case the camera is rotated by an angle φ around axis y, implying the following transformation on (9.12):

$$x \to x\cos\varphi - z\sin\varphi \tag{9.22}$$

giving

$$\left(x\cos\varphi - z\sin\varphi - X_C\right)^2 + \left(y - Y_C\right)^2 = R^2 \tag{9.23}$$

The expression of the intersection between the cylinder and the laser plane, projected onto the camera plane is found in the same way as (9.16). One has:

$$\left(x\cos\varphi + \left(y\tan\delta - e\right)\sin\varphi - X_C\right)^2 + \left(y - Y_C\right)^2 = R^2 \tag{9.24}$$

Coordinate Y_1 is simply $Y_C - R$, allowing us to replace Y_C in (9.24), while $X_{2'}$ and $X_{3'}$ are again at the intersection between the straight line $y = Y_1$ and the two tangents to curve (9.24), passing by the origin of the WCS. Their equations are

$$y = T_{\varphi,j}\,x \tag{9.25}$$

where $j = 2$ or 3, depending on the tangent being considered.

The expression of $T_{\varphi,j}$ is obtained in the same way as (9.19), but to guarantee the symmetry of the laser curve around the optical axis—simulating a centered aim—one must have $T_{\varphi,2} = T_{\varphi,3}$, implying a constraint on X_C. One finds:

$$X_C = \left(Y_1 \tan\delta - e + \frac{RY_1 \tan\delta}{Y_1 + R} \right) \sin\varphi \tag{9.26}$$

so that $T_{\varphi,j}$ can be written as:

$$T_{\varphi,j} = \pm\frac{Y_1 + R}{R}\sqrt{\frac{Y_1\,(Y_1 + 2R)}{Y_1 \tan^2\delta\,(Y_1 + 2R)\sin^2\varphi + (Y_1 + R)^2}}\cos\varphi \tag{9.27}$$

or, as δ is generally very small:

$$T_{\varphi,j} \cong \pm\frac{\sqrt{Y_1\,(Y_1 + 2R)}}{R}\cos\varphi \tag{9.28}$$

We then have:

$$X_{2'} = -\frac{Y_1}{T_{\varphi,2}} \;;\; X_{3'} = \frac{Y_1}{T_{\varphi,3}} \tag{9.29}$$

and expression (9.4) provides us with the erroneous R_φ resulting from the "three-tangent method." The relative error ρ_φ made on the measurement eventually is:

$$\rho_\varphi = \frac{R_\varphi - R}{R} \tag{9.30}$$

It is symmetrical around $\varphi = 0$ and depends on R, Y_1, e and δ.

9.6.5 Analysis of the relative error

Fig. 9.10 shows the relative error on the radius versus angles θ and φ, in an examplative case (e = 10 cm, $\delta = 3°$, R = 15 cm and Y_1 = 1.5 m), if the cylinder slant is not taken into account.

We see that angle φ has the most significant influence on the measurement accuracy, this being noticeable as soon as the tilt value is higher than a few degrees. This clearly proves the need of a generalization of the method.

Angle θ is less critical as the relative error remains below 1% until 20 degrees of tilt angle, but we have to take it into account as well.

The difference between those two effects was predictable: a tilt along axis x (angle φ) drastically lengthens the laser curve, resulting in a significant positive error on R, while a tilt along axis y (angle δ) does not sensibly modify its length, but just its shape.

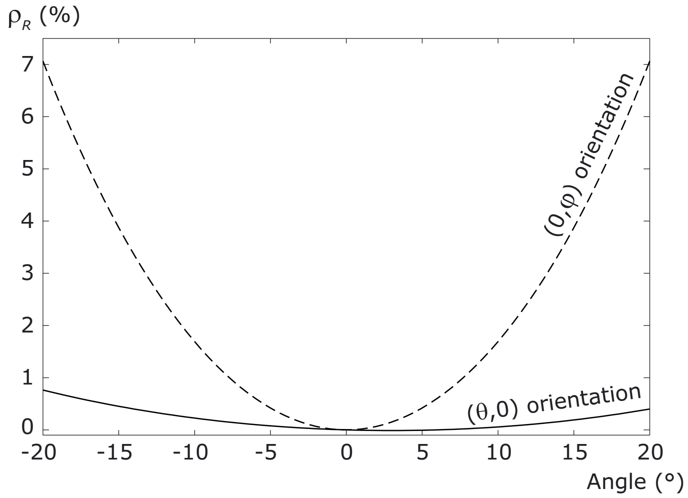

Fig. 9.10. Relative error ρ_R on R if the cylinder slant is not taken into account. $R = 15$ cm and $Y_1 = 1.5$ m.

9.7 Generalization to a Randomly Tilted Cylinder

Let the cylinder under test have the arbitrary orientation defined on Fig. 9.9 with regard to the (x, y) plane of the camera (still supposed horizontal for convenience) observing the scene.

The perfectly cylindrical object is, this time, illuminated by two laser planes (still generated by a specific line generator placed at the exit of a laser diode) slightly tilted in the y direction on the camera plane, creating two curved lines on the object (see Fig. 9.11). We will further justify the laser plane duplication.

We again suppose that the portion of the cylinder illuminated by each laser plane is at least equal to that seen by the camera. The narrow-band interference filter is still present in front of the camera's objective.

In the case of a vertical cylinder, one laser plane only was sufficient to determine the radius. To determine the cylinder orientation in the general case of a tilted axis (cf. Section 9.10), two planes are needed, and the result will depend on thirteen parameters: the same seven for the camera and six for the laser planes (see Fig. 9.12 and Chapter 3). Distances e_1 and e_2, tilt angles δ_1 and δ_2 and the zoom factor of the camera are chosen with the same consideration as in Section 9.2. For additional interpretation of Fig. 9.12, see also Fig. 9.13.

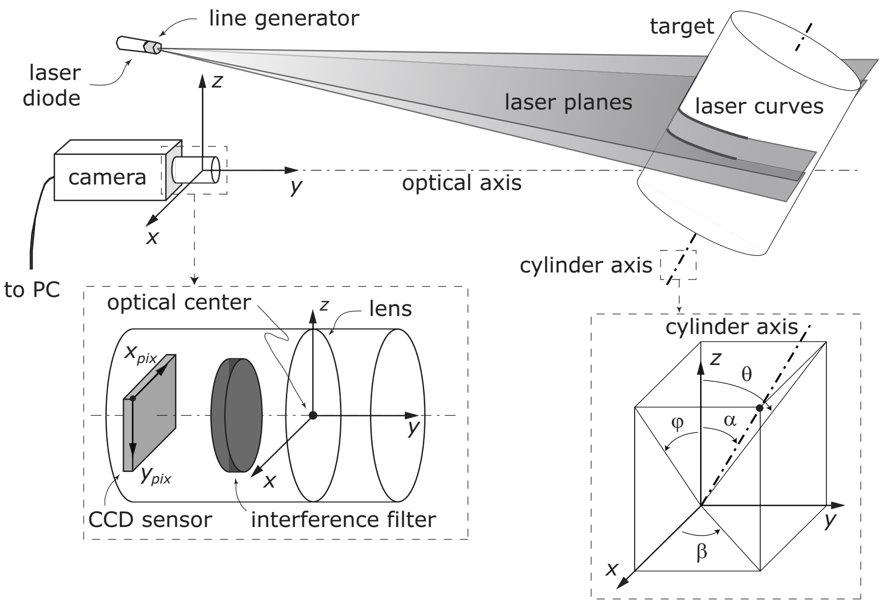

Fig. 9.11. Configuration of the device. 3-D view. Case of a randomly tilted cylinder.

The two distinct procedures described in Chapter 6 are again used to calibrate the instrument, the laser plane calibration being still performed on known cylindrical objects (again, the latter can obviously not be performed until the generalized radius calculation method has been chosen; see Sections 9.8–9.10).

The same image processing algorithm extracts the characteristics of the laser curves necessary to the object radius determination, by isolating them from the rest of the scene.

9.8 Equation of the Laser Curve in the General Case

Generalizing the problem to a cylinder of random orientation has the effect on the geometry of the three-tangent problem that the projection onto the camera plane of the intersection between the laser plane i and the cylinder is not a circle anymore ($i = 1$ or 2, denoting the considered laser plane).

It actually becomes an ellipse, with its long axis $R_{x',i}$ rotated by an angle λ_i from axis x (cf. Fig. 9.13—its short axis is noted $R_{y',i}$; we suppose $X_{3',i} > X2', i)$. To prove it, we will express the equation of the laser curve in the WCS.

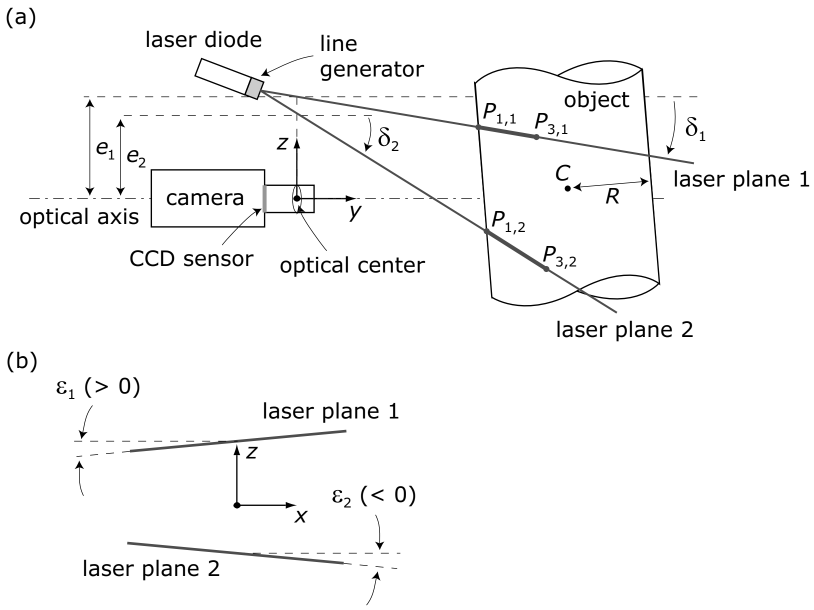

Fig. 9.12. Geometry of the device in the generalized case. (a) Cut in the vertical plane (y, z). (b) Cut in the vertical plane (x, z).

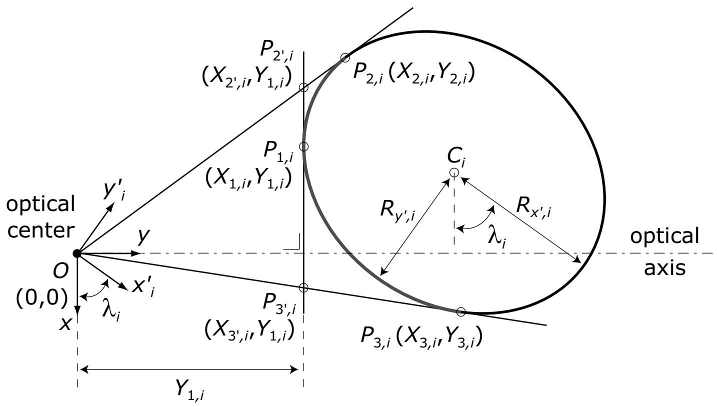

Fig. 9.13. Ellipse. View in the camera plane.

Starting with an orthogonal coordinate system having one of its axes coinciding with the cylinder axis, we will firstly determine the equation of the randomly tilted cylinder in a system aligned with the WCS (but not sharing the same origin), by way of successive rotations of the axes. The intersection between the laser plane and the object will then give us the expression of the laser curve.

Let (x^{IV}, y^{IV}, and z^{IV}) be the original orthogonal coordinate system, with z^{IV} passing by the cylinder axis [see Fig. 9.14(a)]. In that system, the equation of the object is

$$x^{IV\,2} + y^{IV\,2} = R^2 \tag{9.31}$$

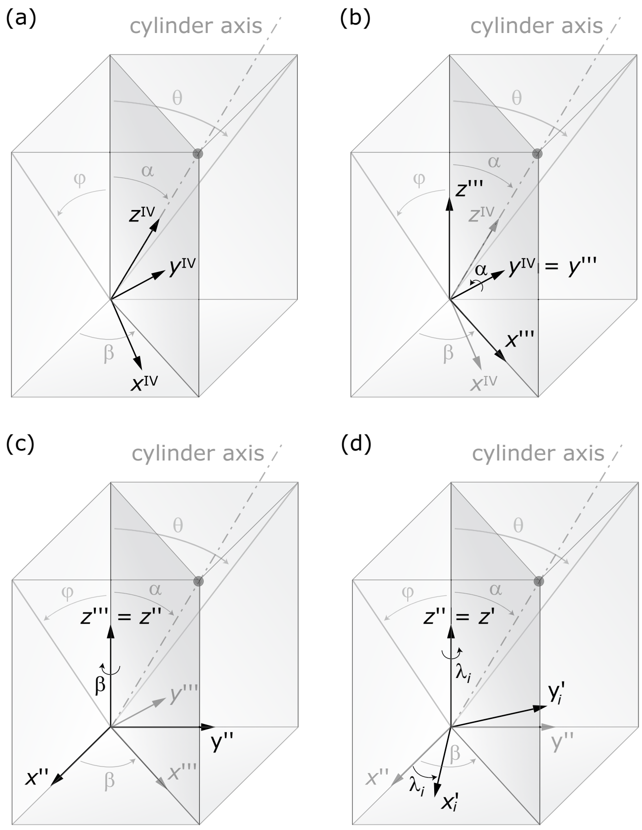

Fig. 9.14. Cylinder axis orientation. Definition of the different coordinate systems.

We call (x''', y''', and z''') the previous system rotated by an angle α around y^{IV} [see Fig. 9.14(b)]:

$$\left\{\begin{array}{lcl} x^{IV} & = & x''' \cos\alpha - z''' \sin\alpha \\ y^{IV} & = & y''' \\ z^{IV} & = & x''' \sin\alpha + z''' \cos\alpha \end{array}\right. \tag{9.32}$$

The equation of the cylinder in that system is

$$(x''' \cos\alpha - z''' \sin\alpha)^2 + y'''^2 = R^2 \tag{9.33}$$

The coordinate system (x'', y'', and z'') is the previous one rotated by an angle β around z''', and is thus aligned with the WCS [but does not share the same origin; see Fig. 9.14(c)]:

$$\left\{\begin{array}{lcl} x''' & = & x'' \cos\beta + y'' \sin\beta \\ y''' & = & -x'' \sin\beta + y'' \cos\beta \\ z''' & = & z'' \end{array}\right. \tag{9.34}$$

We can thus describe the cylinder by

$$((x'' \cos\beta + y'' \sin\beta)\cos\alpha - z'' \sin\alpha)^2 + (x'' \sin\beta - y'' \cos\beta)^2 = R^2 \tag{9.35}$$

Laser plane i is described by (3.5), which becomes, abstraction made of the axis origin:

$$x'' \tan\epsilon_i + y'' \sin\delta_i + z'' \cos\delta_i = 0 \tag{9.36}$$

The expression of the intersection between the cylinder and laser plane i, projected onto (x'', y'') is thus [elimination of z'' in (9.35) and (9.36)]:

$$\begin{array}{c} \left(x'' \left(\cos\beta\cos\alpha + \frac{\tan\epsilon_i \sin\alpha}{\cos\delta_i}\right) + y'' \left(\sin\beta\cos\alpha + \tan\delta_i \sin\alpha\right)\right)^2 \\ + (x'' \sin\beta - y'' \cos\beta)^2 = R^2 \end{array} \tag{9.37}$$

The laser curve is thus well an ellipse, of equation

$$A_i x''^2 + 2B_i x'' y'' + C_i y''^2 = R^2 \tag{9.38}$$

where

$$\left\{\begin{array}{ll} A_i = & \left(\cos\beta\cos\alpha + \frac{\tan\epsilon_i \sin\alpha}{\cos\delta_i}\right)^2 + sin^2\beta \\ B_i = & \left(\cos\beta\cos\alpha + \frac{\tan\epsilon_i \sin\alpha}{\cos\delta_i}\right)(\sin\beta\cos\alpha + \tan\delta_i \sin\alpha) \\ & -\cos\beta\sin\beta \\ C_i = & (\sin\beta\cos\alpha + \tan\delta_i\sin\alpha)^2 + cos^2\beta \end{array}\right. \tag{9.39}$$

Coefficients A_i, B_i and C_i depend on the laser plane orientation (δ_i, ϵ_i), determined through the calibration procedure, and on the cylinder tilt angles (α, β), whose expressions will be calculated in Section 9.10. The ellipse is consequently perfectly known.

In the following paragraph, for sake of clarity, we don't note the suffix i identifying the laser plane anymore.

9.9 Radius Calculation: the Generalized "Three-Tangent Method"

The laser curve, transposed in the image plane, has fundamentally the same characteristics than in the transversal case. It is thus pertinent to still apply the "three-tangent method" for the radius calculation in the generalized case, the problem being now to find an ellipse from the three tangents $OP_{2'}$, $OP_{3'}$ and $P_1P_{3'}$, the latter being oriented in the x (or similarly x'') direction.

By means of a few manipulations on the ellipse, it is possible to keep the same formula as (9.4) for the radius determination. For that, we have at first to know the orientation λ of the ellipse and the expressions $R_{x'}$ and $R_{y'}$ of its axes.

Let us define a new coordinate system (x', y', and z') as [see Fig. 9.14(d)]:

$$\left\{\begin{array}{lcl} x'' & = & x'\cos\lambda - y'\sin\lambda \\ y'' & = & x'\sin\lambda + y'\cos\lambda \\ z'' & = & z' \end{array}\right. \tag{9.40}$$

The ellipse is aligned with this new system, and its equation may thus not contain any term in $x'y'$. This implies from (9.38):

$$\tan 2\lambda = \frac{2B}{A-C} \tag{9.41}$$

giving the expression of angle λ.

In the same system, the ellipse is written:

$$\frac{x'}{R_{x'}}^{2} + \frac{y'}{R_{y'}}^{2} = 1 \tag{9.42}$$

where

$$\begin{array}{lcl} R_{x'}^2 & = & \frac{2R^2}{A+C+\mathrm{sign}(A-C)\sqrt{(A-C)^2+4B^2}} \\ R_{y'}^2 & = & \frac{2R^2}{A+C-\mathrm{sign}(A-C)\sqrt{(A-C)^2+4B^2}} \end{array} \tag{9.43}$$

giving the expression of the two axes of the ellipse.

It is easy to verify that in the particular case of a vertical cylinder ($\alpha = 0$), we find again a circular projection ($R = R_{x'} = R_{y'}$).

In order to have the possibility to use the same genre of formula than (9.4), let us define the coordinate system (x^*, y^*) obtained by a proper scaling followed by a given rotation on (x', y'):

$$\begin{cases} x^* &= R\left(\frac{x'}{R_{x'}}\cos\omega - \frac{y'}{R_{y'}}\sin\omega\right) \\ y^* &= R\left(\frac{x'}{R_{x'}}\sin\omega + \frac{y'}{R_{y'}}\cos\omega\right) \end{cases} \tag{9.44}$$

The scaling operation transforms the ellipse into a circle of radius R, but changes the orientation of tangent $P_1P_{3'}$ (cf. Fig. 9.13) with x^* as well. A rotation by an angle ω is thus needed, with

$$R_{y'}\tan\omega = R_{x'}\tan\lambda \tag{9.45}$$

to ensure the realignment of $P_1P_{3'}$ with x^*.

We are thus put back to the same situation as in Section 9.4, i.e. finding a circle that is tangent to three given lines, one of them being aligned with x^*. Note that this coordinate transformation does not alter the tangent status of lines $OP_{2'}$, $OP_{3'}$ and $P_1P_{3'}$.

We will use the same relation as (9.4):

$$R = \frac{Y_1^*\left(X_{3'}^* - X_{2'}^*\right)}{\sqrt{X_{2'}^{*\,2} + Y_1^{*\,2}} + \sqrt{X_{3'}^{*\,2} + Y_1^{*\,2}} - \left(X_{3'}^* - X_{2'}^*\right)} \tag{9.46}$$

where the superscript * means that the coordinates are expressed in the (x^*, y^*) system. Radius R, in the case of a randomly tilted cylinder, is thus determined with the same robust coordinates Y_1, $X_{2'}$ and $X_{3'}$ than in the transversal case, guaranteeing a very good accuracy.

Applying this computing sequence to both laser planes provides us with similar results. Taking the average of the two calculated radius values permits us to increase the accuracy on the radius.

The last step is the determination of the cylinder orientation, constituting the very need of having a second laser plane.

9.10 Determination of the Cylinder Orientation

The two laser planes provide us with two sets of three tangents, as defined on Fig. 9.13—namely $OP_{2,1}$, $OP_{3,1}$ and $P_{1,1}P_{3',1}$ for the first laser plane and $OP_{2,2}$, $OP_{3,2}$ and $P_{1,2}P_{3',2}$ for the second. Grouped by pairs, those tangents define three planes tangent to the cylinder (see Fig. 9.15):

- π_1, formed by $P_{1,1}P_{3',1}$ and $P_{1,2}P_{3',2}$ and parallel to axis x;
- π_2, formed by $OP_{2,1}$ and $OP_{2,2}$ and passing by the optical center;
- π_3, formed by $OP_{3,1}$ and $OP_{3,2}$ and passing by the optical center.

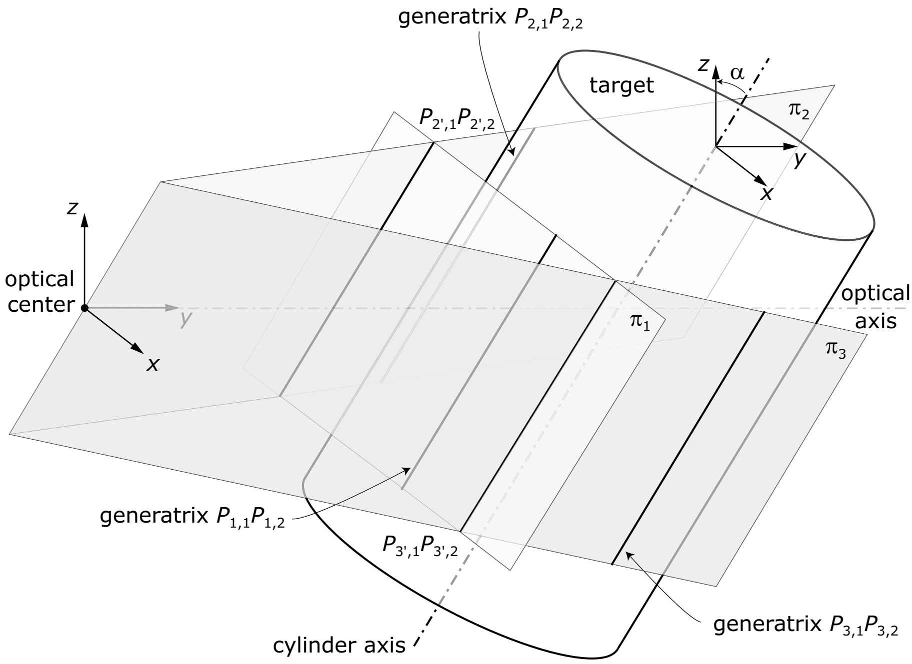

Fig. 9.15. Determination of the cylinder orientation. 3-D view.

This construction defines three generatrices parallel to the object axis (see Fig. 9.15). None of them can however be determined with a satisfactory accuracy, as we have shown in Section 9.5 that abscissas of $P_{1,1}$ and $P_{1,2}$ and ordinates of $P_{2,1}$, $P_{2,2}$, $P_{3,1}$ and $P_{3,2}$ can be highly erroneous.

To determine the cylinder orientation, we will rather use the property that the two straight lines at the intersections of π_1 with π_2 and π_3, i.e. $P_{2',1}P_{2',2}$ and $P_{3',1}P_{3',2}$, are also parallel to the cylinder axis. They are moreover deduced from partial coordinates accurately known (cf. Section 9.5).

One easily sees that (see Fig. 9.16)

$$\begin{aligned} \tan\alpha &= \frac{\sqrt{\left(X_{2',1}-X_{2',2}\right)^2+(Y_{1,1}-Y_{1,2})^2}}{Z_{1,1}-Z_{1,2}} \\ &= \frac{\sqrt{\left(X_{3',1}-X_{3',2}\right)^2+(Y_{1,1}-Y_{1,2})^2}}{Z_{1,1}-Z_{1,2}} \end{aligned} \tag{9.47}$$

($\alpha \geq 0$ as $Z_{1,1} > Z_{1,2}$). Angle β is determined in the (x, y) plane, where one has:

$$\begin{aligned} X_{2',1} - X_{2',2} \geq 0 \rightarrow \beta \quad &= \arctan \tfrac{Y_{1,1}-Y_{1,2}}{X_{2',1}-X_{2',2}} \\ &= \arctan \tfrac{Y_{1,1}-Y_{1,2}}{X_{3',1}-X_{3',2}} \\ X_{2',1} - X_{2',2} < 0 \rightarrow \beta \quad &= \pi + \arctan \tfrac{Y_{1,1}-Y_{1,2}}{X_{2',1}-X_{2',2}} \\ &= \pi + \arctan \tfrac{Y_{1,1}-Y_{1,2}}{X_{3',1}-X_{3',2}} \end{aligned} \tag{9.48}$$

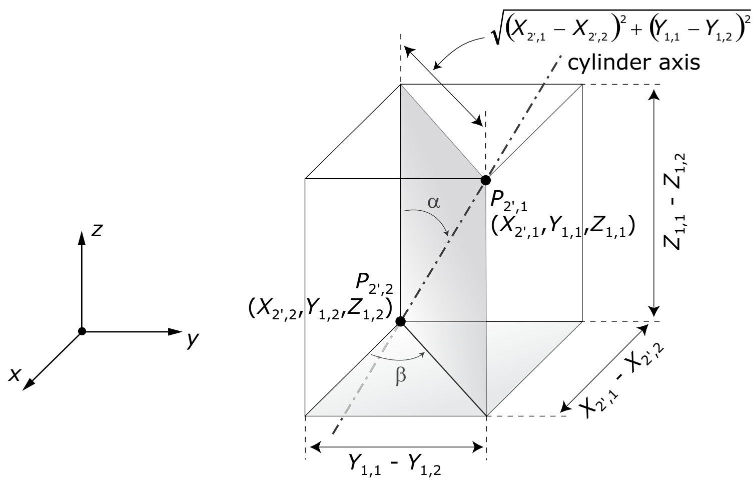

Fig. 9.16. α and β calculation. 3-D view.

Note that the use of both expressions for each formula (9.47) and (9.48) enhances the accuracy on the angles by taking the average of the two values.

Angles α and β are thus deduced from the same robust coordinates than the ones used for the radius calculation, namely $Y_{1,i}$, $X_{2',i}$ and $X_{3',i}$. The only difference is that they have to be determined for both laser planes.

In the image plane, the quantities to measure are shown on Fig. 9.17.

9.11 Expected Accuracy

An analytical study of the accuracy on the radius that one can expect, in a similar way than in Chapter 7, would be very tedious in the general case. It is nevertheless possible to estimate it on the simple case of a centered cylinder having its axis transversal to the camera plane.

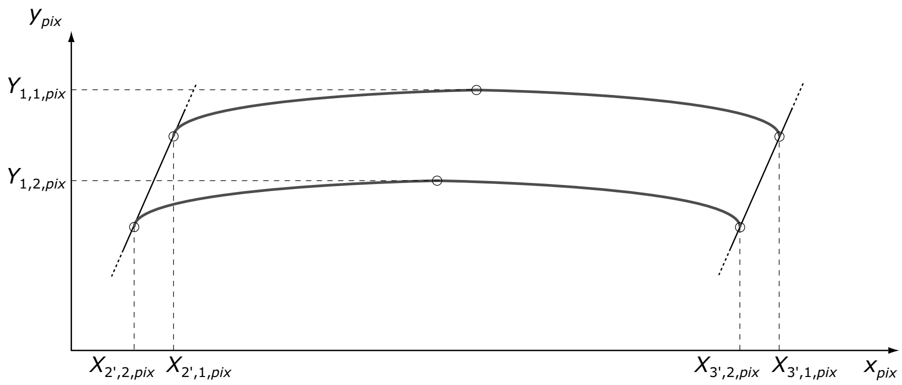

Fig. 9.17. Quantities to measure on the laser curves. View in the image plane.

In this case, the radius R is calculated by (9.4) where $X_{3'} = -X_{2'}$. Using (7.1)—i.e. we make the same suppositions than in Chapter 7 regarding γ and ϵ— this expression becomes:

$$R = \frac{e x_{pix,2'} \left(x_{pix,2'} - \sqrt{x_{pix,2'}^2 + f_x^2} \right)}{f_x \left(y_{pix,1} + f \tan \delta \right)} \tag{9.49}$$

where $x_{pix,2'}$ is the ICS abscissa of $X_{2'}$ and $y_{pix,1}$ the ICS ordinate of Y_1.

The relative error ρ_R on the radius can be estimated by using the partial derivatives of R with regard to the different parameters:

$$\begin{aligned} \rho_R \quad = \quad & \left| \frac{\partial R}{\partial y_{pix,1}} \frac{\Delta y_{pix}}{R} \right| + \left| \frac{\partial R}{\partial x_{pix,2'}} \frac{2\Delta x_{pix}}{R} \right| + \\ & \left| \frac{\partial R}{\partial e} \frac{e\rho_e}{R} \right| + \left| \frac{\partial R}{\partial f_x} \frac{f_x \rho_{f_x}}{R} \right| + \left| \frac{\partial R}{\partial \tan\delta} \frac{\tan\delta \rho_\delta}{R} \right| \end{aligned} \tag{9.50}$$

where the values of all the parameters (R excepted) and uncertainties are as defined in Chapter 7 (case 1), and the factor 2 in front of Δx_{pix} takes into account the fact that two abscissas are normally to be identified in the uncentered case (it is indeed pertinent since the partial derivatives of R with regard to $x_{pix,2'}$ and $x_{pix,3'}$ are identical).

Without entering into the analytical details allowing to solve (9.50), we can announce that a total relative error ρ_R of 1.2% is obtained, for $R = 0.1$ m and $Y_1 = 1$ m (distance). The major contributions come from the errors on $x_{pix,2'}$ (0.93%) and on $y_{pix,1}$ (0.12%).

One could conclude that the hoped accuracy of 1% is impossible to reach, but this figure of 1.2% has been obtained by considering the worst of the cases, i.e. when the errors terms have their maximum values and the same sign (either positive or negative). Is is therefore likely that the experimental error will be sensibly lower, and thus possibly below 1%.

Of course, this development does not apply to the general case of a randomly tilted cylinder. However, as no additional quantities are required to be measured on the image, compared to the particular situation studied hereabove, we can expect a similar accuracy. This will actually be corroborated by our experiments in the next section.

9.12 Results

9.12.1 Introduction

A PC-connected pre-prototype was used, composed of Camera #1 (see TABLE 4.1), Lens #1 (see TABLE 4.2) and Laser #2 (see TABLE 4.3).

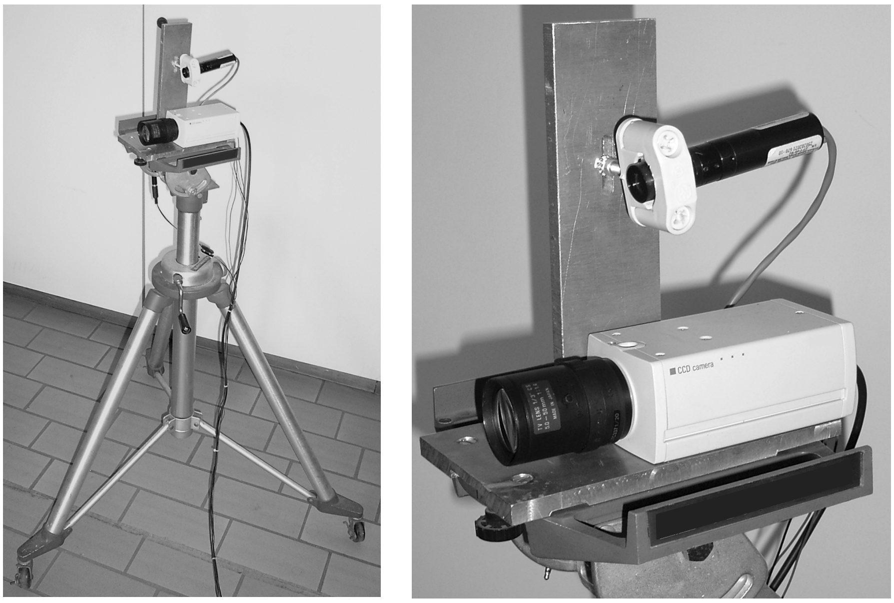

Fig. 9.18. Photograph of the instrument. Left image shows a global view of the instrument mounted on a tripod, while right picture presents a close-up of the camera and the laser diode.

The camera calibration procedure gave us parameter values similar to those obtained in Section 6.2.2, the distortion coefficients excepted (they are almost multiplied by a factor ten). This is due to the fact that the interference filter, placed in the front of the CCD sensor during calibration, raises the distortion level (there was no filter when we proceeded to the camera calibration in Section 6.2.2).

Two-line generators being unavailable on the market, we worked with three laser planes, which allowed us to raise the accuracy on the radius by taking the average of the multiple results.

Vertical distances e_i were fixed to about 10 cm and tilt angles δ_i to 0.5°, 2°and 3.5°respectively.

As a matter of example, Fig. 9.19 gives the photograph of a typical scene acquired by the camera. The cylinder is placed in a clear room, in front of a wall. The raw image, obtained before the processing, is on the left. The efficacy of the interference filter is perceptible. The additional lines of lower luminance are due to a grating effect of the laser optics, generating superior diffraction orders. These lines, together with the segments out of the cylinder, disappear after data processing (right image).

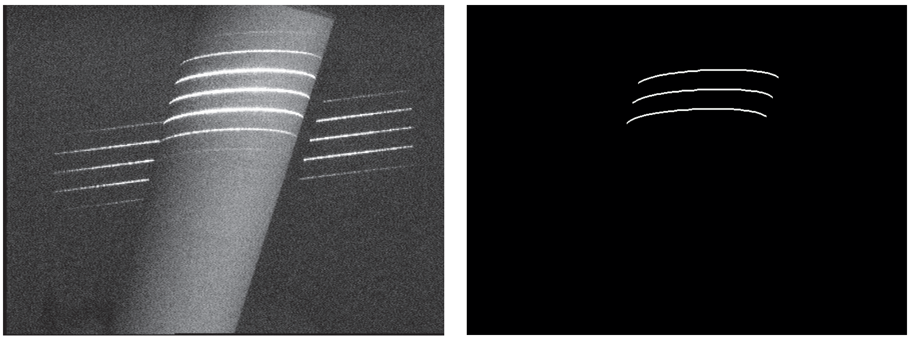

Fig. 9.19. Example of observed scene. The raw image is on the left, the same picture after image processing being on the right.

A flexible steel measuring tape, of accuracy class II, was used to determine the radii of the cylinders used to make the experiments. According to [48], this ensures an accuracy of 0.5 mm on the circumference. We can thus estimate that the "ground truth" on the radii is guaranteed with an accuracy of 0.1 mm ($\approx 0.5/2\pi$).

9.12.2 Transversal cylinders

We firstly made a measurement campaign, in a clear room, of 49 experiments on 7 cylindrical objects transversal to the camera plane, of various radii (from 5 to 15 cm), and for different distances between the optical center of the camera and the target (50 cm to 2 m). The results are fully conclusive as in 94% of the cases, the relative error ρ_R on the radius is below 1% (cf. Fig. 9.20). For other recapitulative figures, see Table 9.2, where the two first lines present the percentage of measurements for which $|\rho_R|$ is below 1 and 1.5% respectively, ρ denotes a relative error and σ a standard deviation.

At this point it is important to specify that strictly speaking, the figures on *all the recapitulative tables presented in this chapter and the following ones* do not represent a *statistical* summary of the performances of the instruments, since they are not calculated on results obtained in identical conditions (distance, diameter, orientation, ... vary). This is why we opted for naming them *recapitulative* figures.

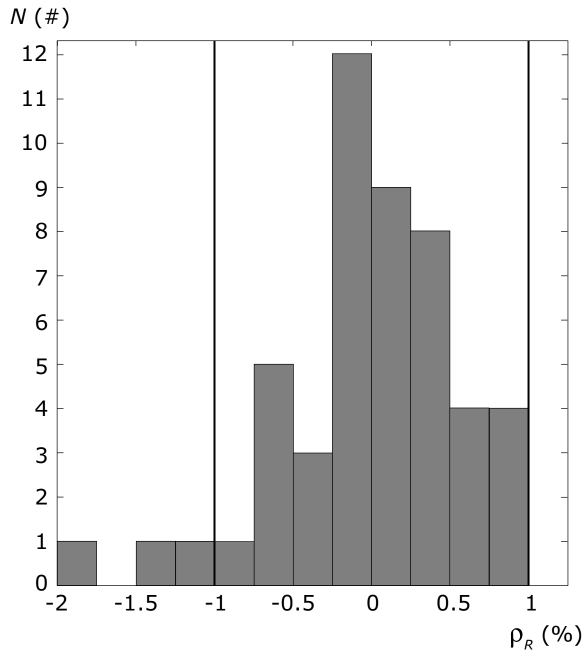

Fig. 9.20. Histogram of the relative error on the radius for transversal cylinders. Forty-nine measurements were performed on seven cylinders, for seven distances.

In the previous section, we calculated the theoretical accuracy on the measurements in the case of a transversal cylinder. The fact that our experiments show a better accuracy than the "pessimistic" 1.2% confirms our intuition that some error terms compensate with each other.

It is to be noted that the three measurements for which the relative error ρ_R on the radius is above 1% were taken on two large objects, at a short distance. The laser lines were so light near the edges of the object that the image processing algorithm could not correctly extract the laser curves (the angular aperture of the laser line generator was too small).

On Fig. 9.21 we present the results of 7 measurements on a 5-cm-radius transversal cylinder, at different distances (50 cm to 2 m). We see that the

TABLE 9.2. Measurement Campaign's Recapitulative Figures for Transversal Cylinders

$\|\rho_R\| < 1\%$	94%
$\|\rho_R\| < 1.5\%$	98%
$\|\rho_R\| < 2\%$	100%
$\rho_{R,\text{mean}}$	-0.05%
σ_{ρ_R}	0.56%

relative error ρ_R is below 1% in any case, and also seemingly independent from the distance. This may look abnormal at the first place, but it is explained by the fact that other causes of error are actually predominant regarding the "distance effect." This phenomenon will be observed in all the experiments presented in Chapters 9–11. Its justification will thus not be repeated.

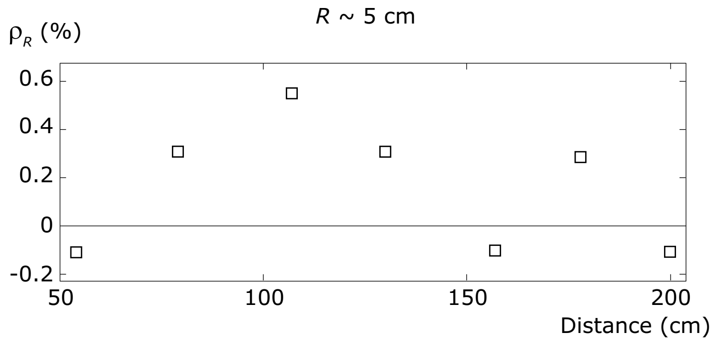

Fig. 9.21. Results of measurements taken on a transversal cylinder at seven distances.

9.12.3 Empirical error committed if the cylinder slant is not taken into account

We then made measurements on a 15-cm-radius cylinder, tilted in particular directions, to check experimentally if the error made on the radius if the cylinder slant is not taken into account was as calculated in Section 9.6. The measurements were made at a distance of 1.5 m between the object and the optical center of the camera. The results obtained for a $(\theta, 0)$ orientation are shown on Fig. 9.22(a), while the $(0, \varphi)$ results are on Fig. 9.22(b). On each figure are also presented in continuous stroke the theoretical errors.

One sees on Fig. 9.22(a) that, the uncertainty on the measurements being of the order of the theoretical error, it is not possible to give a pertinent interpretation of the results. However, this somehow proves that angle θ is not critical in the radius calculation.

Fig. 9.22(b) clearly shows the correspondence between theory and practice, and the need to take the cylinder orientation into account. At first sight, one could think that it would not be necessary for angle θ, but even if it is the case when $\phi = 0$, it is uncertain that it will still be when $\phi \neq 0$. We will therefore include angle θ in our calculations. (The determination of the cylinder orientation provides us with both angles anyway.)

9.12.4 Randomly tilted cylinders

The next and most important step is a measurement campaign, still in a clear room, of 400 experiments on 8 cylindrical objects of various radii (from 5 to 15 cm), distances to the instrument (1 m and to 2 m) and tilts (up to 20°for both θ and φ; this value could appear as moderate, but as they increase, the angles make the measurement harder as it is becoming more and more difficult to keep the whole laser lines in the camera sensor field).

The results are again fully conclusive as in 92% of the cases, the relative error ρ_R on the radius is below 1% (cf. Fig. 9.23). For other recapitulative figures, see TABLE 9.3, where the two first lines present the percentage of measurements for which $|\rho_R|$ is below 1 and 1.5% respectively, ρ denotes a relative error, σ a standard deviation and Δ an absolute error. Left column completes the results of Fig. 9.23, while right one gives figures related to the performances obtained on the cylinder orientation estimation. We observe that the accuracy on θ is poorer than on φ. The consequence of it is not serious, as we showed in Section 9.6 that θ is less critical than φ.

TABLE 9.3. Measurement Campaign's Recapitulative Figures in the Generalized Case

$\lvert\rho_R\rvert < 1\%$	92%	$\Delta\varphi$mean	$-0.3°$
$\lvert\rho_R\rvert < 1.5\%$	98%	$\sigma_{\Delta\varphi}$	2.3°
$\lvert\rho_R\rvert < 2\%$	100%	$\lvert\Delta\varphi\rvert < 5°$	98%
$\rho_{R,}$mean	0.006%	$\Delta\theta$mean	2.2°
σ_{ρ_R}	0.59%	$\sigma_{\Delta\theta}$	4.7°
		$\lvert\Delta\theta\rvert < 10°$	94%

On Fig. 9.24 we present the results of 50 measurements on a 5-cm-radius cylinder, for two distances (1 m and 2 m), five θ angles and five φ angles. We clearly see that the relative error ρ_R is independent from the cylinder

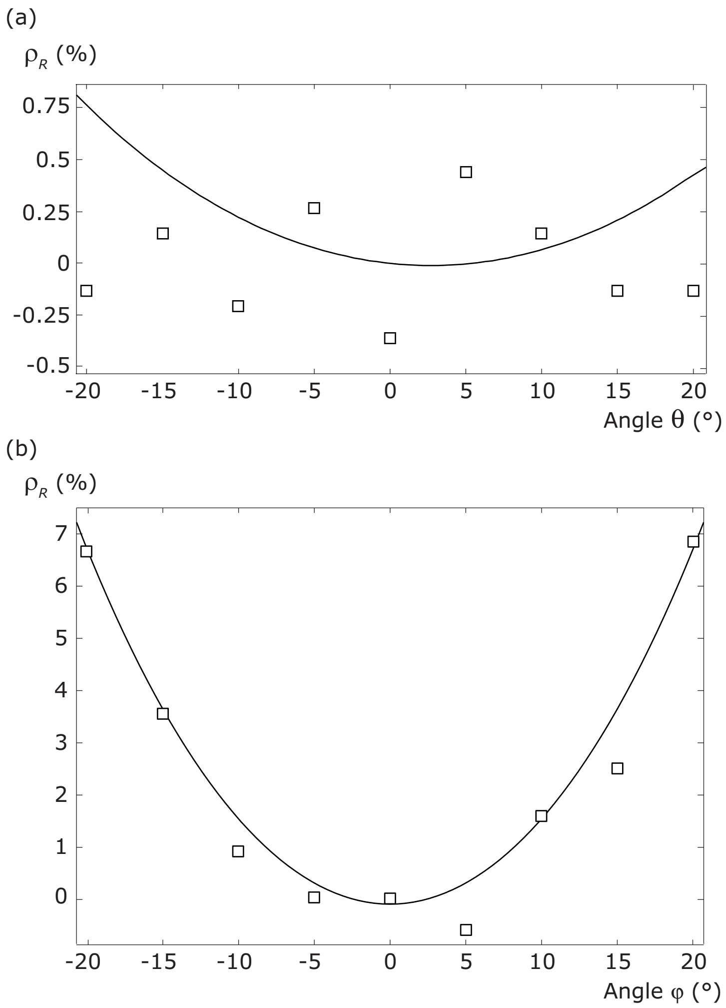

Fig. 9.22. Error committed if the cylinder slant is not taken into account and comparison with the theoretical calculation. (a) Case of a $(\theta, 0)$ orientation. (b) Case of a $(0, \varphi)$ orientation.

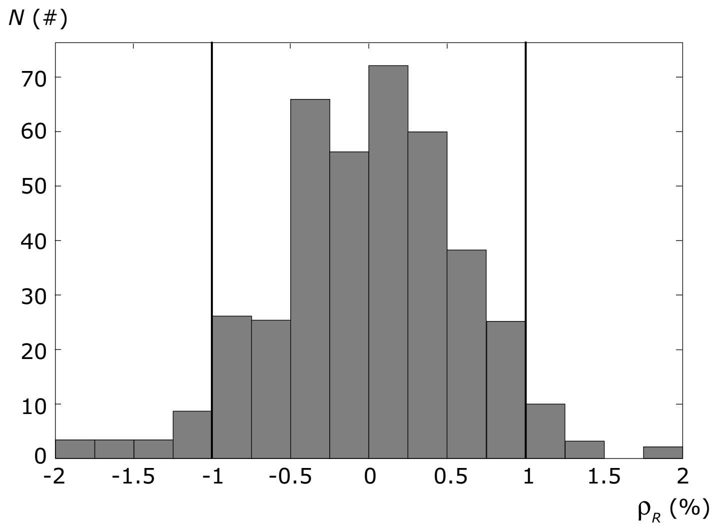

Fig. 9.23. Histogram of the relative error on the cylinder radius in the generalized case. Four hundreds measurements were performed on eight cylinders, for twenty-five orientations and two distances.

orientation, this being a consequence of the fact that our method is analytically exact.

These results confirms our supposition expressed in Section 9.11 that the achievable accuracy on randomly tilted cylinders is of the same order than on transversal cylinders, because no additional quantities are to be measured on the image, but also because the final value of R is the average of 3 different measurements (one per laser plane).

9.12.5 Limits of the instrument

We finally made some measurements to figure out the limitations of our instrument. At first, we tried to measure a 15-cm-radius cylinder at distances greater than 2 meters. As one sees on Fig. 9.25, the results are still satisfactory until 3.5 meters, This figure would of course go smaller with the radius.

We then tried to measure two cylinders whose radii where below 5 cm (about 3 and 1.25 cm). The results remain good until a distance of about 1.3 meters, as shown on Fig. 9.26.

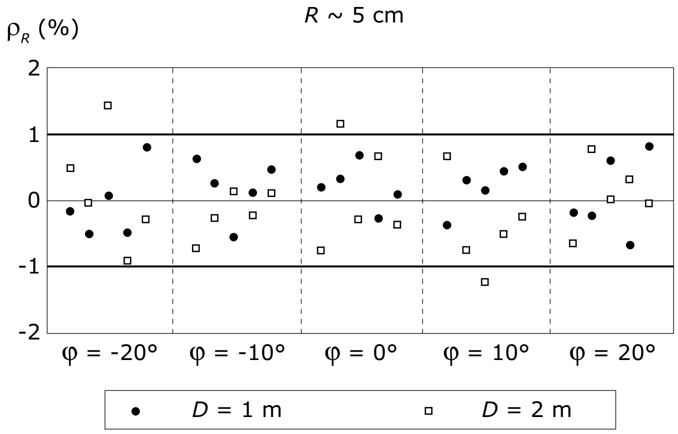

Fig. 9.24. Results of measurements taken on a cylindrical object at two distances, in the generalized case. Each φ area contains five columns at different θ values ($-20°$, $-10°$, $0°$, $10°$and $20°$from left to right).

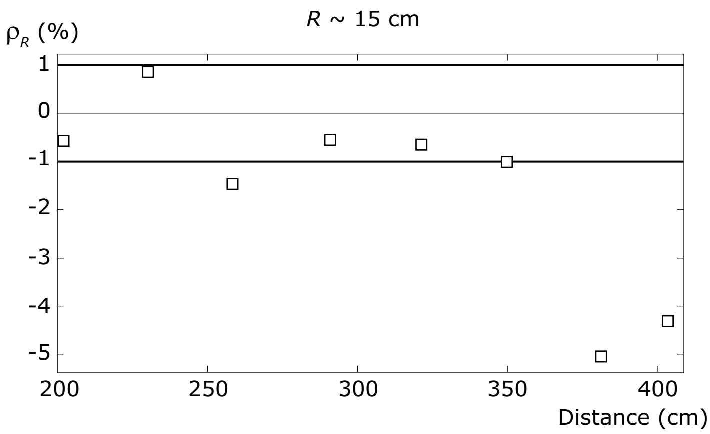

Fig. 9.25. Results of measurements taken on a cylindrical object at distances greater than 2 m.

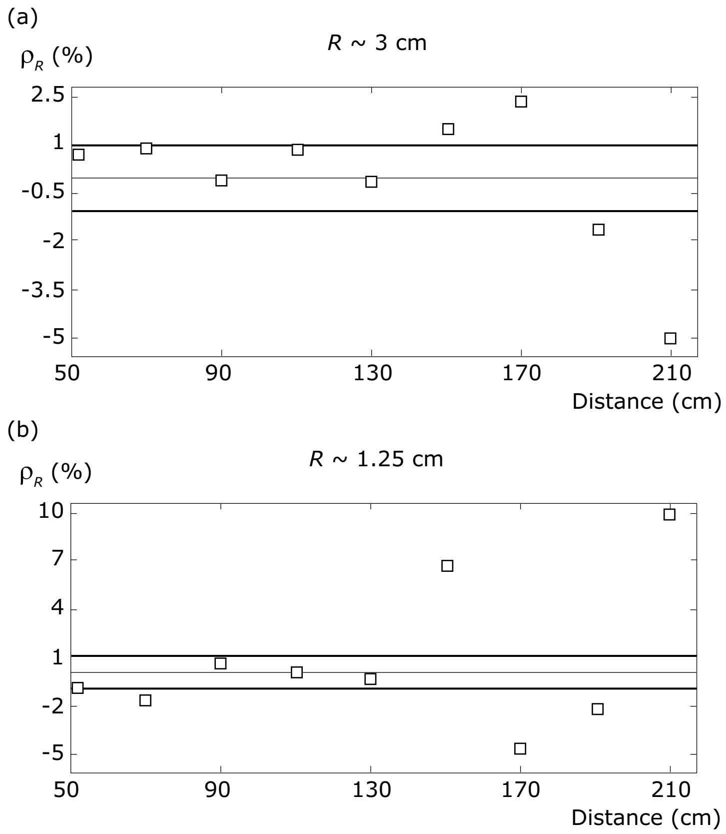

Fig. 9.26. Results of measurements taken on cylindrical objects, the radii of which are smaller than 5 cm. (a) 3-cm-radius cylinder. (b) 1.25-cm-radius cylinder.

9.12.6 Influence of the camera imperfections

One could wonder which results would be obtained if the imperfections of the camera (i.e. the skewness factor γ and the two distortion coefficients k_1 and k_2) were not taken into account.

At first, we observed that—as expected—γ being so low, it does not have any influence on the results ($\Delta R_{\max} = 1\ \mu$m).

Secondly, if the distortion is not corrected (we remind the reader that it is significant seen the presence of an interference filter), we observe a raise on each result of about 0.5% (mean value). This figure appears as rather low, especially if we consider the fact that the displacement of a pixel because of distorsion can go up to 11 pixels at the edges of the image. Because of the negative value of the distortion coefficients, the pixels at the extremities of the laser lines are considered as further away from their centers, compared to their actual undistorted position. The immediate consequence is an overestimation of the radius, but it is partly compensated by the fact that the ordinates of the centers of the curves are also overestimated (when those points are above the center of the image, which was true in the majority of the cases), i.e. the object is considered as closer to the instrument than it actually is.

9.13 Without a Refined Theory...

As explained in the general introduction of the thesis, we opted for grouping in Part I all the theoretical aspects related to the various devices developed in Part II.

It is therefore necessary to explicitly emphasize how each application is linked with Part I, and particularly which negative consequences we would have had to face if the theoretical models were not so refined.

For this particular application, the following observations can be made:

- Chapter 2: a simpler camera model would lead to unacceptable errors, as previously shown in Section 9.12.6;
- Chapter 3: obviously, (3.7) relating a 2-D point in the image to its corresponding 3-D point in the WCS, is a prerequisite. To be fair, the value of angle ϵ is so low that it could have been neglected, without sensibly depreciate the quality of the results. However, it is easy to include it in the calculations (and in the calibration procedure), so we preferred to take it into account. Generally speaking, if the user does not pay as much attention as we did to ensure that $\epsilon \cong 0$, it makes sense to include it in the model;

- Chapter 5: regarding image processing, one can point out (beside all the essential operations allowing to extract the laser curves) that without subpixel location, the error would have been drastically higher (probably multiplied by 3, which was shown as the improvement ratio provided by the algorithm; see Section 5.7.1). Curve smoothing is critical as well in the case of trees (to eliminate the bark protuberances), but not in the case of a perfect cylinder;
- Chapter 6: if the calibration procedure was not so robust (repeatability of about 0.1%), we would of course have obtained worst results.

These remarks lead to the conclusion that without such a complete theoretical basis, one would never have reached such good performances.

9.14 Conclusions

The feasibility of a new method for the diameter measurement of cylindrical objects was studied. Beyond the forest domain, this application opens several industrial prospects, such as inaccessible pipe measurement and quality control.

The innovative character of our instrument is to be found in the patented "three-tangent method," for the robust determination of the radius of a circle.

We showed that it is the best computation method taking into account the characteristics of the laser curve, and we generalized it to the ellipse, corresponding to the case of a cylinder of any orientation (θ, φ).

We claim a general accuracy of about 1% on the diameter of the measured objects of any orientation, for diameters ranging from 10 to 30 cm and for a distance—a priori not known—between the instrument and the cylindrical object going up to 2 m. These figures are in perfect agreement with the industrial needs expressed in Section 9.1.2. They are valid for a camera objective of fixed focal length of about 8 mm and a distance between the camera optical center and the laser planes of about 10 cm. Smaller and larger diameters can also be tackled at rated distance ranges.

Note that the study of the PC replacement by an autonomous processing system at low additional cost is currently being done by the Belgian factory WOW Company, intending to produce and commercialize the instrument.

Finally, one could mention the case of a cylinder whose cross section is not exactly circular. Our method would give, as any other would, an erroneous result on the "diameter," depending on the shape of this cross section and on the cylinder orientation with regard to measuring head of the instrument. The first step toward a generalization to the circumference measurement of such objects would be to consider the cross section as elliptic. Combined with a random aim, the problem is complicated and certainly needs multiple aims.

This generalization topic is an open objective, attractive both for its useful purpose and challenging nature!